CRACK GROWTH PREDICTIONS IN A COMPLEX HELICOPTER COMPONENT UNDER SPECTRUM LOADING

J. C. Newman, Jr. [1]
Department of Aerospace Engineering
Mississippi State University
Mississippi State, MS 39762, USA
Tel: 1-662-325-1521 Fax: 1-662-325-7730
Email: j.c.newman.jr @ ae.msstate.edu

P. E. Irving and J. Lin
School of Industrial & Manufacturing Science
Cranfield University
Cranfield, Bedford MK43 0AL
UNITED KINGDOM

Dy D. Le
Federal Aviation Administration
William J. Hughes Technical Center
Atlantic City International Airport
Atlantic City, NJ 08405, USA

ABSTRACT

Fatigue crack growth predictions have been made on a helicopter round-robin crack configuration. The crack configuration was a small corner defect at the edge of a large central hole in a flanged plate made of 7010 aluminum alloy and the component was subjected to a simulated helicopter spectrum loading. The crack growth rate data and the stress-intensity factor solution for the crack configuration were provided in the round robin. The FASTRAN life-prediction code was used to predict fatigue crack growth under various load histories on the aluminum alloy, such as Rotorix and Asterix, on both compact specimens and the complex crack configuration. A BEASY three-

[1] Corresponding author

dimensional stress-intensity factor solution for the round-robin problem was also provided for this paper and is compared with the original K solution. Comparisons are made between measured and predicted fatigue crack growth lives for both crack configurations. The predicted lives for the compact specimens were 15 to 30 percent longer than the measured lives; and crack growth in the round-robin configuration agreed very well in the early stages of crack growth, but the life was 30 percent short of the test results at the final crack length.

Keywords: fatigue, cracks, aluminum alloy, spectrum loading, stress-intensity factor

NOMENCLATURE

B thickness, mm

C_i coefficient in crack growth equation

C_5 cyclic fracture toughness, MPa-$m^{1/2}$

c crack length, mm

F boundary correction factor of stress intensity factor

K_{max} maximum stress intensity factor, MPa-$m^{1/2}$

N cycles

N_e experimental cycles

N_p predicted cycles

n_i power in crack growth equation

q constant in crack growth equation

R stress ratio (S_{min}/S_{max})

r hole radius, mm

S_{max} maximum applied stress, MPa

S_{min} minimum applied stress, MPa

S_o crack opening stress level, MPa

W width, mm

α constraint factor

ΔK stress intensity factor range, MPa-$m^{1/2}$

ΔK_{eff} effective stress intensity factor range, MPa-$m^{1/2}$

σ_{ys} yield stress, MPa

σ_u ultimate tensile strength, MPa

INTRODUCTION

In recent years, there has been a strong interest in applying damage-tolerance procedures to helicopter components. Several international workshops have been organized to review and to study whether these procedures can be effectively applied to high-cycle rotorcraft components. It is widely known that the particular characteristics of rotorcraft materials, loading spectra, and component configurations make the task of predicting crack growth very difficult.

Recently, the helicopter community [1, 2] developed a round-robin challenge problem to benchmark the ability of the industry to predict fatigue crack growth life in a simulated complex helicopter component under rotorcraft spectrum loading to support the use of the damage-tolerance approach. The configuration and initial corner crack dimensions (2-mm radius), crack growth rate data on the aluminum alloy, and the stress-intensity factor solution were provided to a number of participants. The round-robin test results were unknown to the participants. About 60% of the predicted lives were within a factor-of-2 of the test life. However, there were two issues that merit

further study. First, the predicted shape of the crack-length-against-cycles curves did not correctly match that of the test data in any of the predictions. Secondly, there was a large spread of predicted lives with a difference of up to a factor of 50 between the shortest and longest predicted lives. Some calculated inspection intervals were longer than the entire experimental life. All of the predictions were unconservative in the early stages of crack growth, which could have serious ramifications to the selection of inspection intervals.

In 1968, Elber [3] observed that fatigue crack surfaces contact with each other even during tension-tension cyclic loading due to “plasticity-induced” crack closure. This observation and the explanation of the crack-closure phenomenon began to explain many crack growth characteristics. Since the discovery of plasticity-induced fatigue crack closure, several other closure or shielding mechanisms have been identified, such as roughness- and oxide-induced closure. These developments have greatly improved our understanding of the complex interactions that occur during crack propagation under variable-amplitude loading. Several numerical models of plasticity-induced crack closure [4-6] have been developed during the past 25 years to calculate crack-opening stresses under complex load histories.

The present paper is concerned with the application of a plasticity-induced crack-closure model, FASTRAN [7], to study fatigue crack growth under various rotorcraft load histories in an aluminum alloy. The model was based on a strip-yield model concept, but modified to leave plastically deformed material in the wake of the advancing crack. The model includes the influence of “constraint” (plane-stress or plane-strain behavior) on the development of plasticity and crack closure. The model was used to correlate

fatigue crack growth rate data under constant-amplitude loading over a wide range in stress ratios and in crack growth rates from compact specimens. Test results under constant-amplitude loading and past experience with a wide variety of materials and thicknesses were used to help establish the constraint factor used in the model. The model was then used to predict crack growth under simulated rotorcraft load histories, such as the Rotorix [8] spectra applied to compact specimens and the Asterix [9] spectra applied to the complex crack configuration used in a rotorcraft round-robin study. Comparisons are made between measured and predicted crack-length-against-cycles and fatigue crack growth lives on the aluminum alloy under the variety of complex load histories.

MATERIAL AND CRACK CONFIGURATIONS

The material considered in this study is 7010-T73651 aluminum alloy [10]. The yield stress and ultimate tensile strength for the aluminum alloy was 434 and 510 MPa, respectively. Fatigue crack growth rate data on the aluminum alloy was determined from compact specimens using the electrical potential technique under constant-amplitude loading. These data were obtained on specimens 17.5 mm thick and 70 mm wide. Tests were conducted at four stress ratios (R = 0.1, 0.4, 0.7, and 0.9) over a wide range in crack growth rates.

Compact specimens made from the same aluminum alloy were also subjected to various versions of the Rotorix spectrum [8]. Herein, only the results for Rotorix-16 and -32 will be analyzed. Rotorix-16, which has 2 million cycles, was derived from a full rotor-head spectrum. Rotorix-32 is a gated version of Rotorix-16 with the high R ratio small-amplitude cycles removed, which greatly reduces the spectrum to 51,405 cycles.

In May 2002, a helicopter damage tolerance round-robin challenge was initiated (see Refs. 1 and 2). The objective was to compare predicted crack growth lives from various participants on a corner defect (2 mm in radius) at the edge of a large central hole in a flanged plate made of the 7010 alloy, as shown in Figure 1. The flanged plate was subjected to the Asterix [9] rotorcraft spectrum. Participants were supplied with a stress-intensity-factor solution derived from three-dimensional finite-element analyses, the constant-amplitude fatigue crack growth rate data, and the spectrum loading sequence. Asterix represents 190.5 hours of helicopter flight and was composed of 371,610 cycles. Section AA shows the plan form of the tensile loaded component with the large central hole with an integral stiffening ring and two large edge flanges. Section BB shows the test section with the initial 2-mm corner crack (r = 30 mm; w = 66 mm). The various crack-front shapes illustrate the approximate crack shapes as the crack grows from the corner crack to the 25-mm crack. The crack length, c, is measured along the surface. In the corner-crack region, the material thickness is 6 mm, but transitions into a long section of 2-mm-thick material before the crack grows into the large flange. Although the crack configuration is three-dimensional, all analyses in the round robin, and herein, were treated as a two-dimensional crack problem. Issues on what three-dimensional stress-intensity factors to use in the analyses are discussed.

EFFECTIVE STRESS-INTENSITY FACTOR RANGE

Elber's effective stress-intensity factor range [3] was based on linear-elastic analyses and is:

$$\Delta K_{\text{eff}} = (S_{\max} - S_o)\,\sqrt{(\pi c)}\,F \qquad (1)$$

where S_{max} is the maximum applied remote stress, S_o is the crack-opening stress, c is the crack length, and F is the usual boundary-correction factor, which accounts for the influence of boundaries on the stress-intensity factor. The crack-opening stress is calculated from either equations that have been developed under steady-state constant-amplitude conditions or from the FASTRAN life-prediction code [7].

The relationship between ΔK_{eff} and crack growth rate (dc/dN) is expressed in term of a table-lookup procedure with a term to account for fracture. The crack growth relation is:

$$dc/dN = C_i (\Delta K_{eff})^{n_i} / [1 - (K_{max}/C_5)^q] \quad (2)$$

where C_i and n_i are the coefficient and power for multi-linear segments, which forms the baseline relation, K_{max} is the maximum stress-intensity factor, C_5 is the cyclic fracture toughness, and q is a fitted parameter. The fracture term is necessary because linear-elastic stress-intensity factors, in general, are not constant at fracture. Thus, C_5 will vary with crack length and component size. However, because of the thick material considered, C_5 was assumed to be a constant value and was determined from the constant-amplitude fatigue crack growth rate data, as the rates approach infinity.

The life-prediction code FASTRAN uses the effective stress-intensity factor range against crack-growth rate (ΔK_{eff}-rate) relation determined from constant-amplitude data over a wide range in stress ratios and rates. A constraint factor (α) is used in the closure model to simulate the three-dimensional stress state around the crack front. Plane-stress condition is $\alpha = 1$ and plane-strain condition is $\alpha = 3$. Equations have been developed to calculate the crack-opening stress (S_o) as a function of stress ratio (R),

ratio of maximum applied stress level to flow stress (S_{max}/σ_o), and the constraint factor [7].

Herein, FASTRAN Version 3.9 is used to make all life calculations. One feature activated in this model is *K*-analogy. The modified strip-yield model is based on either: (1) a central crack in a finite-width plate or (2) two symmetric cracks emanating from a hole in a finite-width plate. For the compact specimen, model 1 is used; but for the round-robin problem, model 2 is used. For either crack configuration, the crack-opening stresses are calculated from the respective model with an applied remote stress, which matches the "stress-intensity factor" on the crack configuration being analyzed. Stress-intensity factors for the round-robin crack configuration are input in table form with linear interpolation, but extrapolations are not allowed.

CONSTANT-AMPLITUDE LOADING

Compact specimens made from the aluminum alloy [10] were subjected to fatigue cycling at various stress ratios, and these data, ΔK against dc/dN, are shown in Figure 2. Because these data were for a thicker material than the round-robin configuration, additional data from NASGRO [11] for 5-mm-thick material is also shown. Results from the two thicknesses overlay quite well. Test results for the thinner 2-mm thick material were not available.

Crack growth rate data from Irving and Buller [10] on the aluminum alloy were analyzed to determine the ΔK_{eff} rate relation. Because high R ratio data is fully open ($\Delta K = \Delta K_{eff}$), the R = 0.7 data is generally used to establish the ΔK_{eff} against the rate curve over a fairly wide range in rates. Figure 3 shows only the R = 0.7 data, which exhibited a large amount of scatter in the near-threshold regime, and the ΔK_{eff} baseline

curve. But at the high R ratios, the upper region of the rate curve is approaching a fracture condition (K_{max} = C_5 = cyclic fracture toughness). The solid curve shows the results from Equation (2) with C_5 = 52 MPa-m$^{1/2}$ and q = 2. The value of C_5 is generally higher than K_{Ic}, the plane-strain fracture toughness.

Because the specimens were thick (17.5 mm), nearly plane-strain conditions (α = 2.5) were found to give a reasonable correlation of the data. All of the test results for the aluminum alloy are shown in Figure 4(a). The correlation is reasonable at high rates, but show more variation near the threshold regime (low rates), especially for the low R ratio results. For the aluminum alloys, it is suspected that the load-reduction procedure is causing higher thresholds and lower rates in the near-threshold regime [12] due to remote closure, which is not accounted for in the steady-state equations. Figure 4(b) shows the same plot with some of the R = 0.1 and 0.4 data eliminated at lower rates. Again, the solid curves show the results from Equation (2), which simulates the fracture process for the high R ratios fairly well. The open symbols on the ΔK_{eff} rate curve show the table-lookup values for FASTRAN using Equation (2).

SIMULATED HELICOPTER LOAD SPECTRA

Compact specimens and the round-robin crack configuration were subjected to simulated helicopter load spectra, typical of dynamic loading on rotorcraft components. Figures 5(a) and 5(b) show a very small part of some of the loading in the Rotorix-32 and Astrix spectra, respectively. Rotorix-32 is a combination of high and medium R ratio block loading with some low R ratio excursions; whereas, Astrix is an extremely high R ratio spectrum with some negative R ratio excursions.

The FASTRAN code was used to calculate crack-growth lives on compact specimens from an initial crack length to failure under some of the Rotorix spectra. Some typical results of calculated crack-opening stresses are shown in Figure 6(a). This figure shows part of the Rotorix-32 spectrum with the corresponding calculated crack-opening stresses. In the model, the crack-opening stresses are held constant during a crack growth increment (Δc^*), which is 20% of the cyclic plastic zone. But damage is calculated on a cycle-by-cycle basis using Equations (1) and (2). At the high R ratio sequence (about 4200 cycles), the crack is nearly fully open (S_o is close to the minimum stress). But during the lower R sequence (4300 cycles), the crack is partially closed. After the application of an underload, the crack-opening stresses are reduced, but the reduction is delayed due to the size of the Δc^* increment. The use of the Δc^* concept (holding S_o constant for number of cycles) is to maintain a reasonable computational speed for the closure model in the FASTRAN code. (Future versions of FASTRAN may have small values of Δc^* because of the vast improvements that have been made in computer speed.)

Figure 6(b) shows the normalized crack-opening load calculations made on the round-robin crack configuration, early in the crack growth simulation (about 40 flights), under the Astrix spectrum. These results show that the negative R ratio excursions cause lower crack-opening loads, but these values rise as the crack grows and leaves more plastic deformations along the crack surfaces.

Figure 7 shows the comparison of measured [13] and predicted crack growth lives from an initial crack length (c_i = 15.8 mm) to failure on compact specimens made of the thick aluminum alloy and subjected to either Rotorix-16 or -32 spectra. In both cases,

the life-prediction code predicted longer lives (or slower crack growth) than the tests, but the results were within 30 percent of the test results.

ROUND-ROBIN CHALLENGE PROBLEM

The helicopter round-robin challenge problem was a corner defect (2 mm in radius) at the edge of a large central hole in a flanged plate made of the 7010 alloy (see Refs. 1 and 2), and the component was subjected to the Asterix [9] spectrum. The corner flaw was located in a 6-mm-thick part and grew into a thin section (2-mm thick) after about 5 mm of crack growth. The crack grew into an 8-mm-thick flange (perpendicular to the crack direction) after about 28 mm of growth. Although the crack configuration is three-dimensional, the crack was to be considered as a “two-dimensional” crack problem. Because in the round-robin crack-configuration tests, crack lengths and crack-growth rates were measured at the surface of the sample only, and these would be the values that participants were required to calculate. Participants were supplied with the stress-intensity factor solution, as shown in Figure 8 (solid curve). The plot shows the boundary-correction factor, *F*, as a function of the normalized crack length, c/(w-r). (In some references, the boundary-correction factor is referred to as □.) This figure also shows a schematic of one-half of the configuration with an initial corner crack. In the round-robin analysis [2], it was found that the experimental crack length against cycles data were faster, in the early stages of growth, than any of the predictions, suggesting that the supplied stress-intensity factors were too low in this region and/or the crack growth rate data fits in the near threshold regime were causing lower rates than the tests.

Stress-Intensity Factor Solution – Computational Mechanics, Inc. (Dr. Tom Curtin), using the BEASY code [14], made three-dimensional calculations for the round-robin problem. In the current study, rather than use a surface value, it was decided to use the "average" stress-intensity factor from the BEASY analysis, and these results are shown as the dashed curve in Figure 8. A major difference was observed in the 2- to 4-mm crack-size range. Because of this difference, a request was made to generate a solution for a 1-mm corner crack and the "stress-concentration" factor at the edge of the hole (without a crack). The stress-intensity boundary-correction factor for the 1-mm crack was slightly higher than the 2-mm crack size, indicating that the solution was approaching the limiting solution for a small crack at the edge of the hole. Using the stress-concentration factor (2.546) based on the net-section stress, which is the normalizing stress in the *K* equation, the limiting value was calculated from Tada et al. [15] and Newman and Raju [16]. These results are shown in Figure 8 as solid symbols. Thus, it can be concluded that the *K* solution from BEASY is most likely the correct solution to the round-robin crack configuration for the early part of the crack-growth process.

In the BEASY solution, crack shapes that simulate the actual round-robin problem were used in the analyses, see Figure 1 (Section BB). Some typical boundary-correction factors along the crack fronts are shown in Figure 9. The initial corner crack (2-mm radius) was a quarter circular shape and showed the classic variations along the crack front with higher values at the free surfaces. The solid line shows the average value. During the transition from the 6-mm to the 2-mm-thick section, the crack shape was oblique and large variations in the boundary-correction factors along the crack front

were observed. The dashed line, again, shows the average value. For cracks in the 2-mm-thick section (not shown), the crack fronts were straight and the variations were quite small. When the crack grew into the fillet region for the edge flange, a straight crack front was assumed, but the actual crack front was curved (see Fig. 1). Again, the dashed line is the average value.

Figure 10 shows the maximum, average, and minimum values from BEASY as a function of the normalized crack length, *c/(w-r).* The position of the maximum and minimum values, along the crack front, change with crack length as the crack progresses. To use two-dimensional analyses for a three-dimensional crack problem raises issues on what stress-intensity factor to use in the analysis. To adequately address this issue, crack-closure behavior must be considered. In the near surface regions, where stress-intensity factors are generally the highest, plane-stress conditions and higher crack-opening stresses are present. Whereas, in the interior, where stress-intensity factors are generally the lowest, plane-strain conditions and low crack-opening stresses prevail. Thus, from a crack-closure standpoint, the ΔK_{eff} values from the exterior to interior locations may show less difference than the absolute values. Also, the FASTRAN crack-closure model is only a two-dimensional model. For simplicity, only the average *F* values will be used in FASTRAN.

Crack-Length-Against-Flight Calculations – The results of two tests conducted on the round-robin crack configuration are shown in Figure 11 as symbols. FASTRAN Version 3.9 was used to make two predictions. In the first, the dashed curve shows the predicted results made with the original K-solution provided in the round robin. (These particular results were not submitted to the round-robin organizers.) However, these

results are similar to most of the other predictions submitted in the round robin, in that, the predicted shape of the curve does not match the test data, especially in the early stages of crack growth. The predicted results are about a factor-of-2 too long in the early stages of crack growth; but for crack growth in the 2-mm-thick material region, the rate of growth is significantly faster than the test data. (The bar on the figure shows a schematic of the various thickness regions for the round-robin configuration.) Ironically, the crack growth life at the 25-mm location was exceptionally close to the average of the two tests. The second crack growth calculation (solid curve) was made with the BEASY *K*-solution (average) and, here, the early stages of crack growth compared very well with the test data. But, again, the crack growth rates in the 2-mm-thick section were too fast. The final flight hours at the 25-mm location was 30 percent short of the average test results. The dash curve is an estimated extension of the predicted results based on an estimated *K*-solution for larger crack lengths.

Unfortunately, 2-mm-thick fatigue crack growth rate data was unavailable. However, for the thinner material, it is expected that a “lower” constraint factor would be operational, which would give higher crack-opening stresses and longer fatigue-crack-growth lives during this phase. Whether crack growth rate data for the 2-mm-thick material and the lower constraint factor would give better crack growth predictions under the Astrix spectrum must await further studies.

FASTRAN has the capability to conduct a linear-cumulative-damage (LCD) calculation for spectrum loading. It was of interest to see how neglecting retardation/acceleration options in the crack-closure model would affect the crack growth behavior. Figure 12 shows these calculations. The solid curve is the full crack-

closure model using the single-crack solution from BEASY. The dashed curve shows the LCD calculations, which indicates that the spectrum is basically retarding crack growth. Recently, Vaughan and Chang [17] used NASGRO [11] and AFGROW [18] to make life calculations on the round-robin crack configuration. They had results from a BEASY analysis, which had two symmetric cracks in the round-robin configuration instead of a single-crack configuration. The dash-dot curve is their AFGROW results using the two-crack solution, which apparently did not have a retardation/acceleration option activated. The dash-double-dot curve is the corresponding FASTRAN (LCD) calculations also using the two-crack solution. FASTRAN and AFGOW agreed fairly well using the same K-solution and the same fatigue crack growth rate data. The single-crack K solution and the crack-closure model produced a very acceptable life prediction.

CONCLUDING REMARKS

The life-prediction code, FASTRAN, was used to predict fatigue crack growth in the 7010 aluminum alloy under two rotorcraft spectra. Using constant-amplitude data on the material and a plane-strain constraint factor, predicted crack growth lives were within 30 percent of tests conducted on compact specimens under two versions of the Rotorix load spectrum. For the round-robin crack configuration, using the “average” stress-intensity factors from a three-dimensional BEASY analysis, and the same materials data, the crack-length-against-flight-hours agreed very well in the early stages of crack growth. But the model predicted faster crack growth during the thin (2-mm) section. The predicted crack growth life at a crack length of 25 mm was 30 percent

short of two tests conducted under the Astrix helicopter spectrum. But, further study is needed to resolve the crack growth inconsistencies for the thin section.

Although FASTRAN has preformed very well and AFGROW has done quite well in the prediction of the test results, modification of the stress-intensity factor solution will not change the overall scatter (in excess of a factor of 40) in the predicted lives between the various life-prediction codes. Some predicted lives were smaller and others were much larger than the test lives. Prediction of crack-growth lives in helicopters, unlike fixed wing aircraft, require accurate calculations in the near threshold regime of the crack-growth-rate curves, where scatter in material data, small changes in curve fitting, and errors in stress-intensity factor calculations all result in substantial changes in predicted lives. Accurate life calculations under helicopter spectra require more accurate values of stress-intensity factors, material crack-growth-rate data, and load spectra than has been observed with fixed wing aircraft.

REFERENCE

1. Cansdale R and Perrett B (2002). The helicopter damage tolerance round-robin challenge. Workshop on Fatigue Design of Helicopters, University of Pisa, Italy, 12-13 September.
2. Irving P, Lin J and Bristow J (2003). Damage tolerance in helicopters – report on the round robin challenge," American Helicopter Society 59th Annual Forum, Phoenix, AZ, 6-8 May.
3. Elber W (1971). The significance of fatigue crack closure. ASTM STP 486, American Society of Testing and Materials, Philadelphia, PA, 230-242.

4. Budiansky B and Hutchinson J (1978). Analysis of closure in fatigue crack growth. J Appl Mech. **45**, 267-276.
5. Newman J Jr (1981). A crack closure model for predicting fatigue-crack growth under aircraft spectrum loading. ASTM STP 748, American Society of Testing and Materials, Philadelphia, 53-84.
6. de Koning A and Liefting G (1988). Analysis of crack opening behavior by application of a discretized strip yield model. ASTM STP 982, American Society of Testing and Materials, Philadelphia, 437-458.
7. Newman J Jr (1992). FASTRAN II – A fatigue crack growth structural analysis program. NASA Technical Memorandum 104159.
8. A standardised fatigue loading sequence for helicopter main rotorhead structures (Rotorix) (1996). Damage Tolerance Group Report CU/927/N/27, Cranfield University, Department of Trade and Industry Link Contract No. RA/6/30/06.
9. A standardised fatigue loading sequence for helicopter airframe structures (Asterix) (1996). Research Paper RP980, GKN Westland Helicopters, Department of Trade and Industry Link Contract No. RA/6/30/06.
10. Irving P and Buller R (1999). Prediction of fatigue life under helicopter loading spectra for safe life and damage tolerant design. ASTM STP 1332, American Society of Testing and Materials, West Conshohocken, PA, 727-742.
11. NASGRO 4 Reference Manual (2002). Fracture mechanics and fatigue crack growth analysis software. Version 4 (www.nasgro.swri.org).
12. Forth S, Newman J Jr and Forman R (2003). On generating fatigue crack growth thresholds. Int. J. Fatigue. **25** (1) 9-15.

13. Zitounis V (2003). Fatigue crack growth rates under variable amplitude load spectra containing tensile underloads. Cranfield University, Ph.D. Thesis.
14. BEASY - Fatigue and crack growth software. Computational Mechanics, Inc., 25 Bridge Street, Billerica, MA 01821 (www.beasy.com).
15. Tada H, Paris P and Irwin G (2002). The Stress Analysis of Cracks Handbook. American Society of Mechanical Engineers, New York, NY.
16. Newman J Jr and Raju I (1986). Stress-intensity factor equations for cracks in three-dimensional finite bodies subjected to tension and bending loads. Computational Methods in the Mechanics of Fracture, S. N. Atluri, ed., Elsevier, 311-334.
17. Vaughan R and Chang J (2003). Life prediction for high cycle dynamic components using damage tolerance. American Helicopter Society 59th Annual Forum, Phoenix, AZ, 6-8 May.
18. AFGROW Users Guide and Technical Manual (2002). AFRL-VA-WP-TR-2002, Version 4.0005.12.10, J. A. Harter, Air Vehicles Directorate, 2790 D Street, Ste 504, Air Force Research Laboratory, WPAFB OH 45433-7542.

LIST OF FIGURES

Figure 1 – Helicopter round-robin crack configuration.

Figure 2 – Stress-intensity factor against rate for 7010-T73651 aluminum alloy.

Figure 3 – Effective stress-intensity factor against rate for aluminum alloy at R = 0.7.

Figure 4(a) – Effective stress-intensity factor against rate for aluminum alloy at various R ratios.

Figure 4(b) – Effective stress-intensity factor against rate for aluminum alloy eliminating low R ratio load-shedding data.

Figure 5(a) – Typical stress-time history for Rotarix spectrum loading.

Figure 5(b) – Typical stress-time history for Astrix spectrum loading.

Figure 6(a) – Calculated crack-opening stresses during the application of the Rotarix-32 spectrum loading.

Figure 6(b) – Calculated crack-opening stresses during the application of the Astrix spectrum loading.

Figure 7 – Measured and predicted crack-growth lives in compact specimens under the Rotorix spectrum loading.

Figure 8 – Stress-intensity factor solutions for round-robin crack configuration as a function of normalized crack length.

Figure 9 – Distribution of stress-intensity factors along the crack front for various crack lengths in round-robin crack configuration.

Figure 10 – Maximum, average, and minimum stress-intensity factors from BEASY [14].

Figure 11 – Measured and predicted crack-length-against-flights for round-robin problem.

Figure 12 – Comparison of crack-length-against-cycles for round-robin crack configuration using the crack-closure model and linear-cumulative damage calculations.

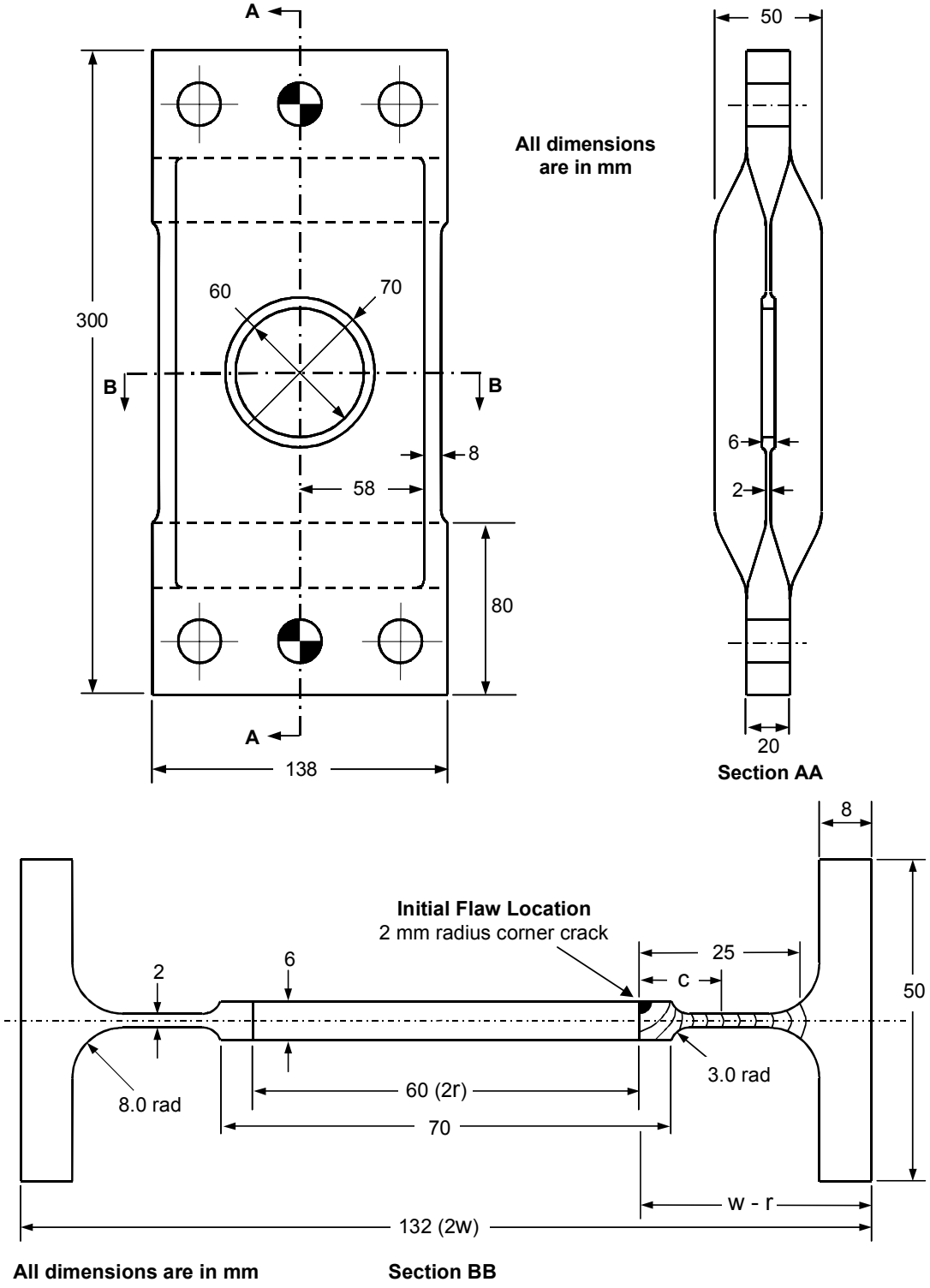

Figure 1 – Helicopter round-robin crack configuration.

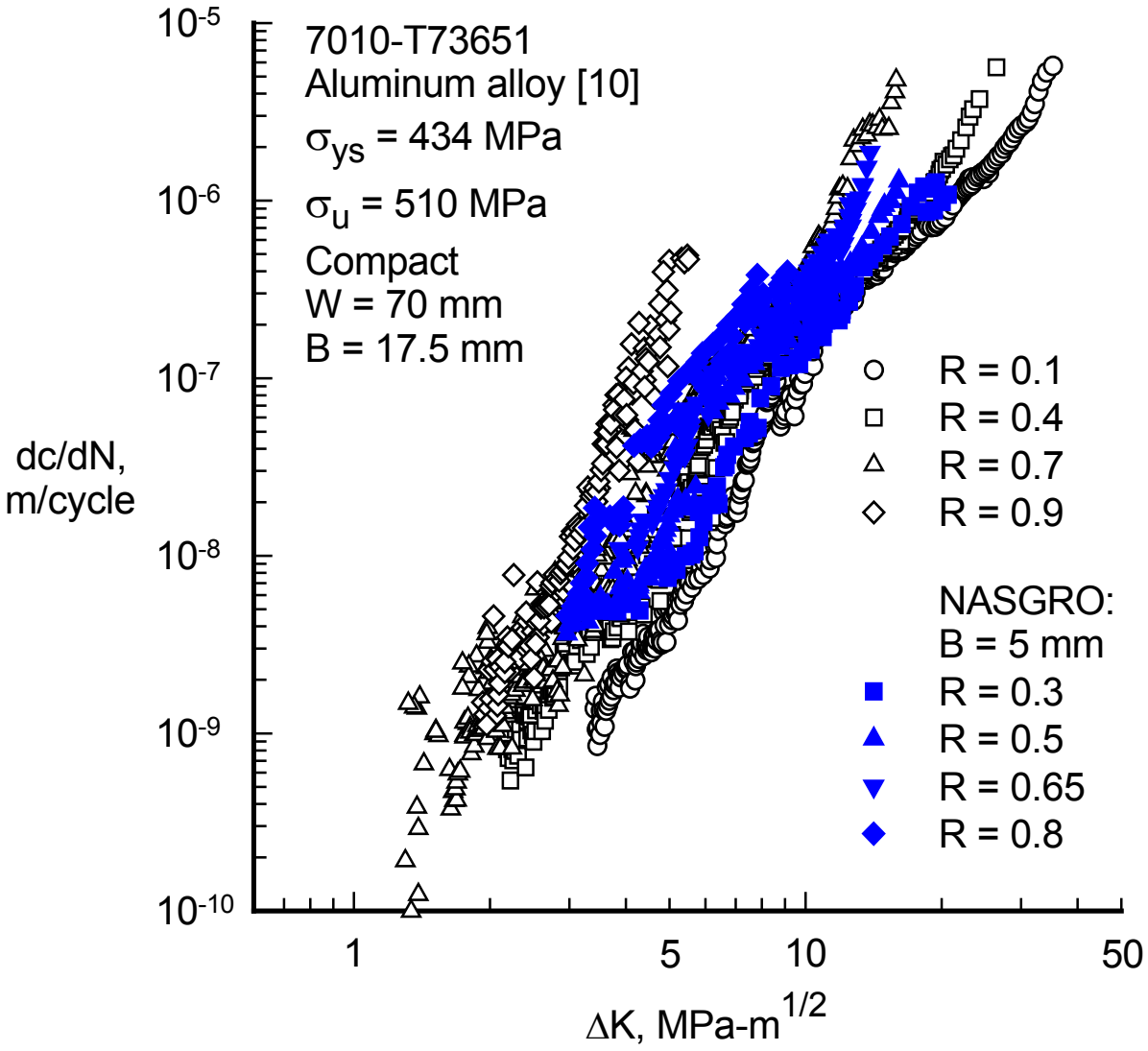

Figure 2 – Stress-intensity factor against rate for 7010-T73651 aluminum alloy.

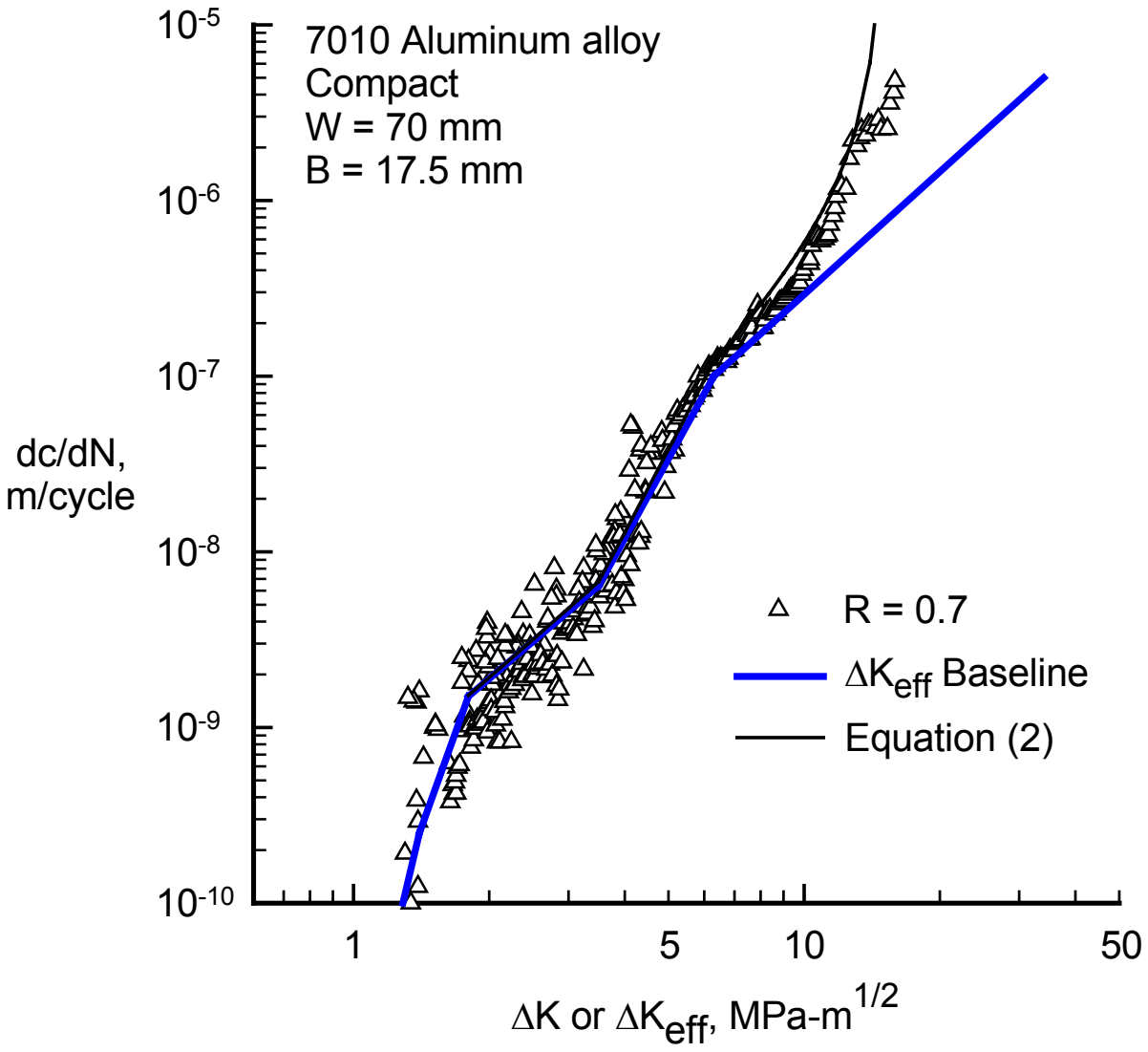

Figure 3 – Effective stress-intensity factor against rate for aluminum alloy at R = 0.7.

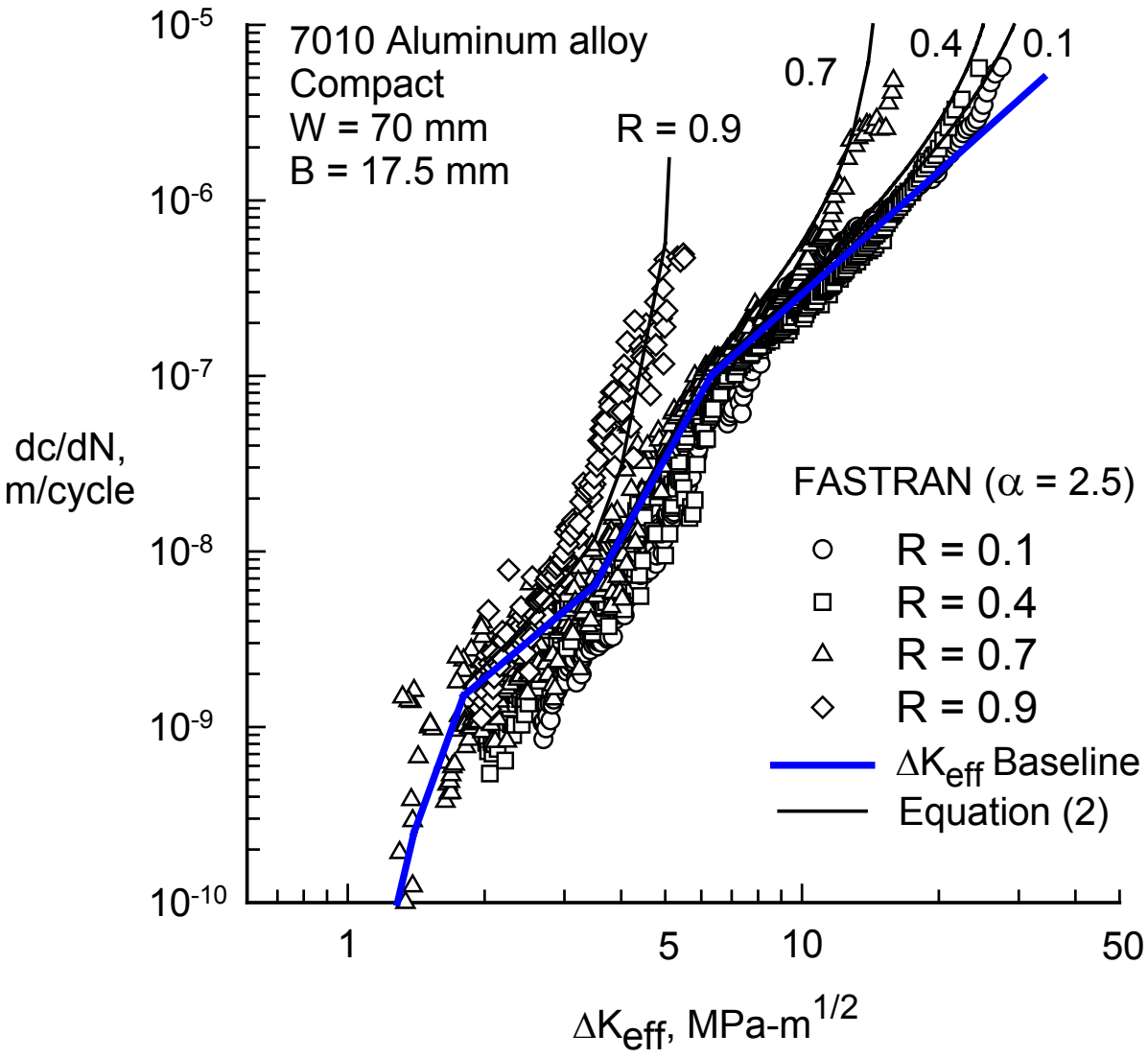

Figure 4(a) – Effective stress-intensity factor against rate for aluminum alloy at various R ratios.

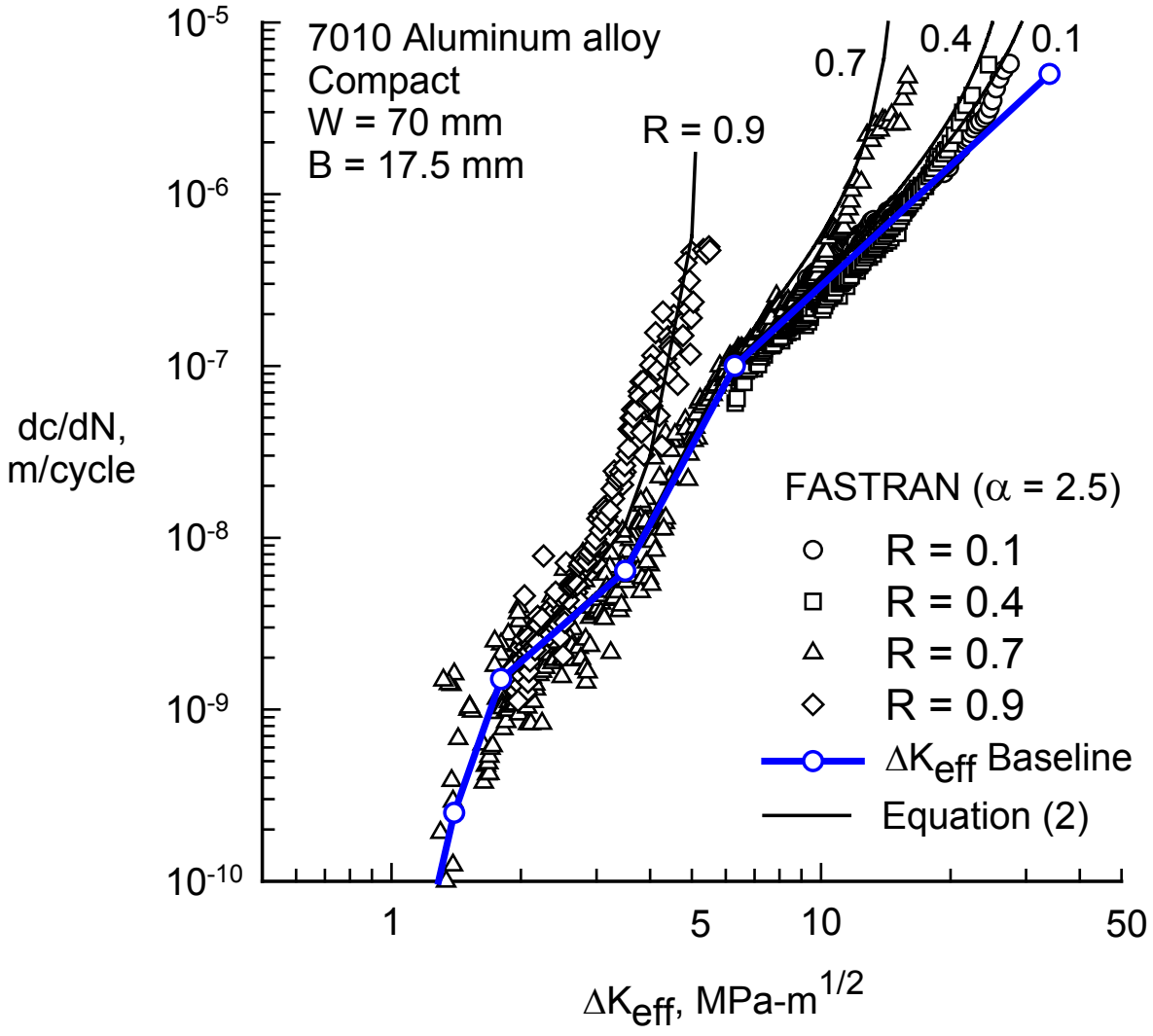

Figure 4(b) – Effective stress-intensity factor against rate for aluminum alloy eliminating low R ratio load-shedding data.

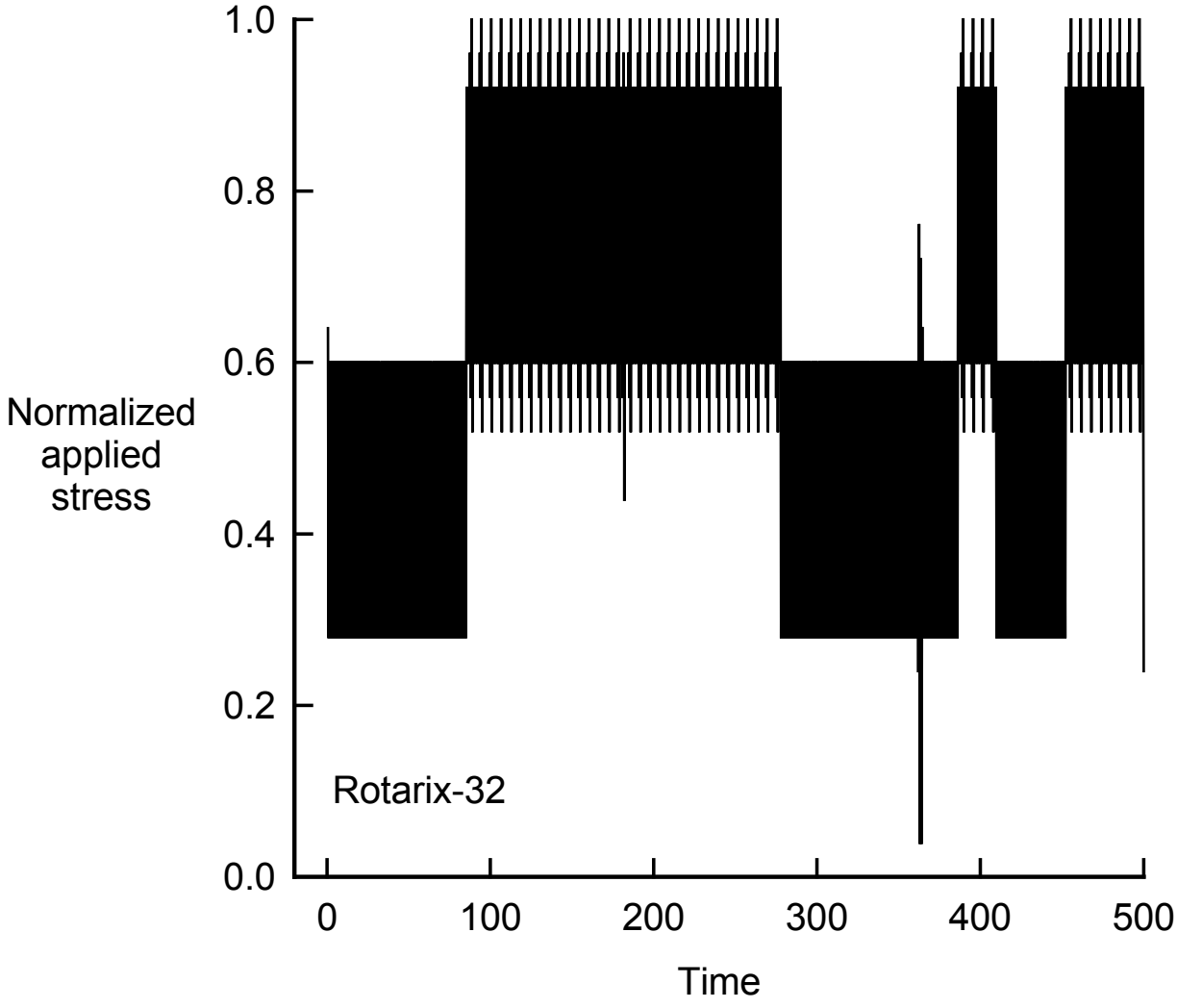

Figure 5(a) – Typical stress-time history for Rotarix spectrum loading.

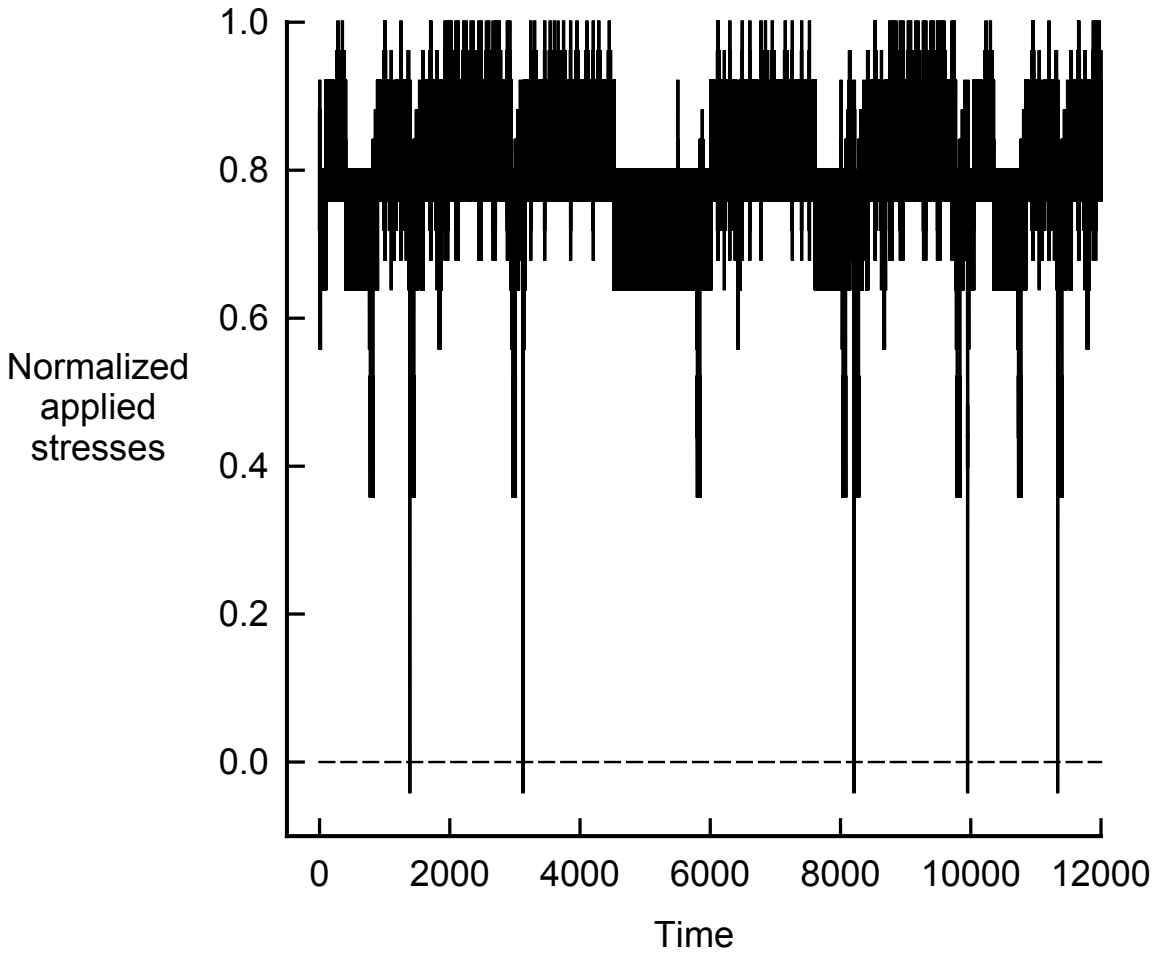

Figure 5(b) – Typical stress-time history for Astrix spectrum loading.

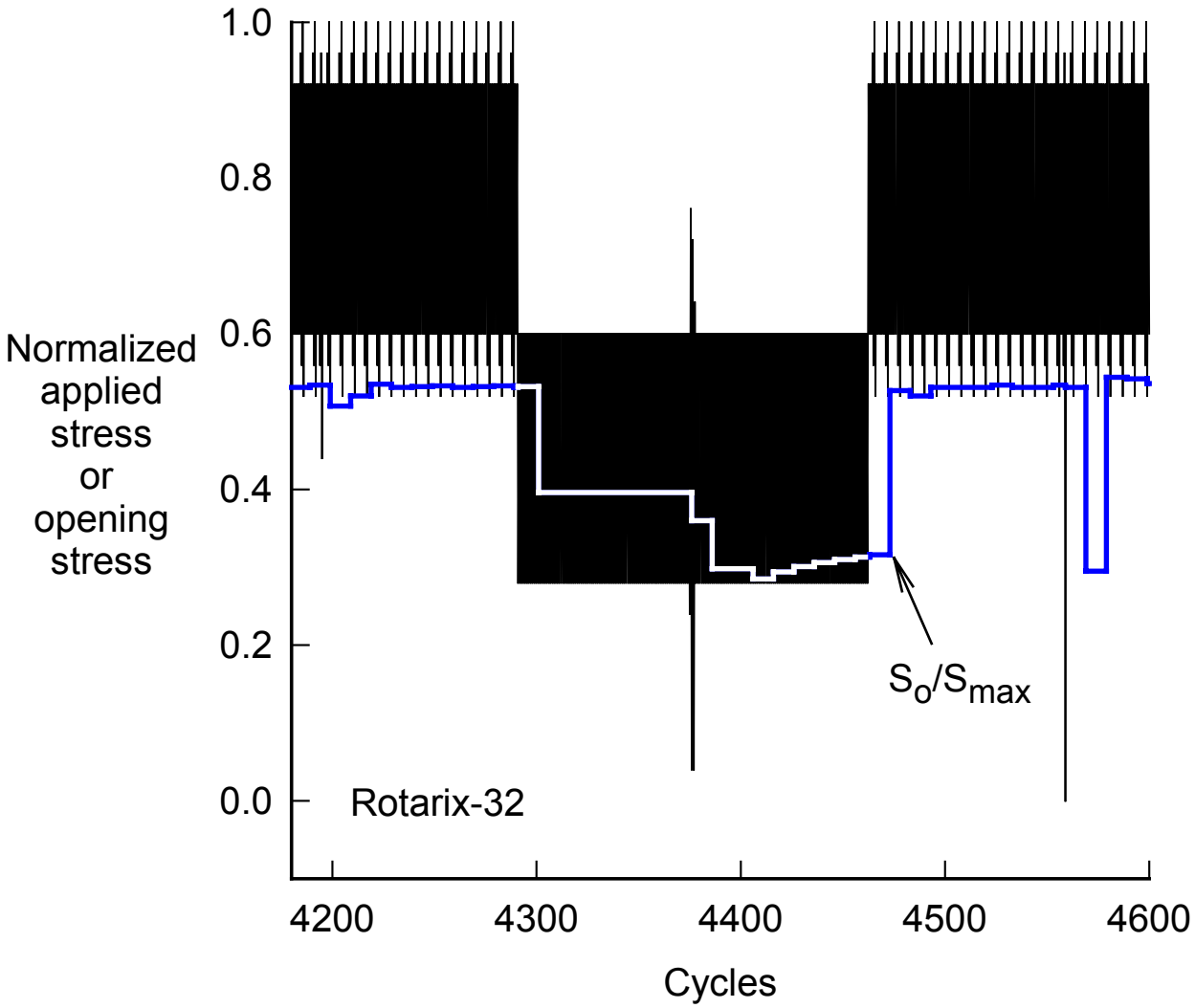

Figure 6(a) – Calculated crack-opening stresses during the application of the Rotarix-32 spectrum loading.

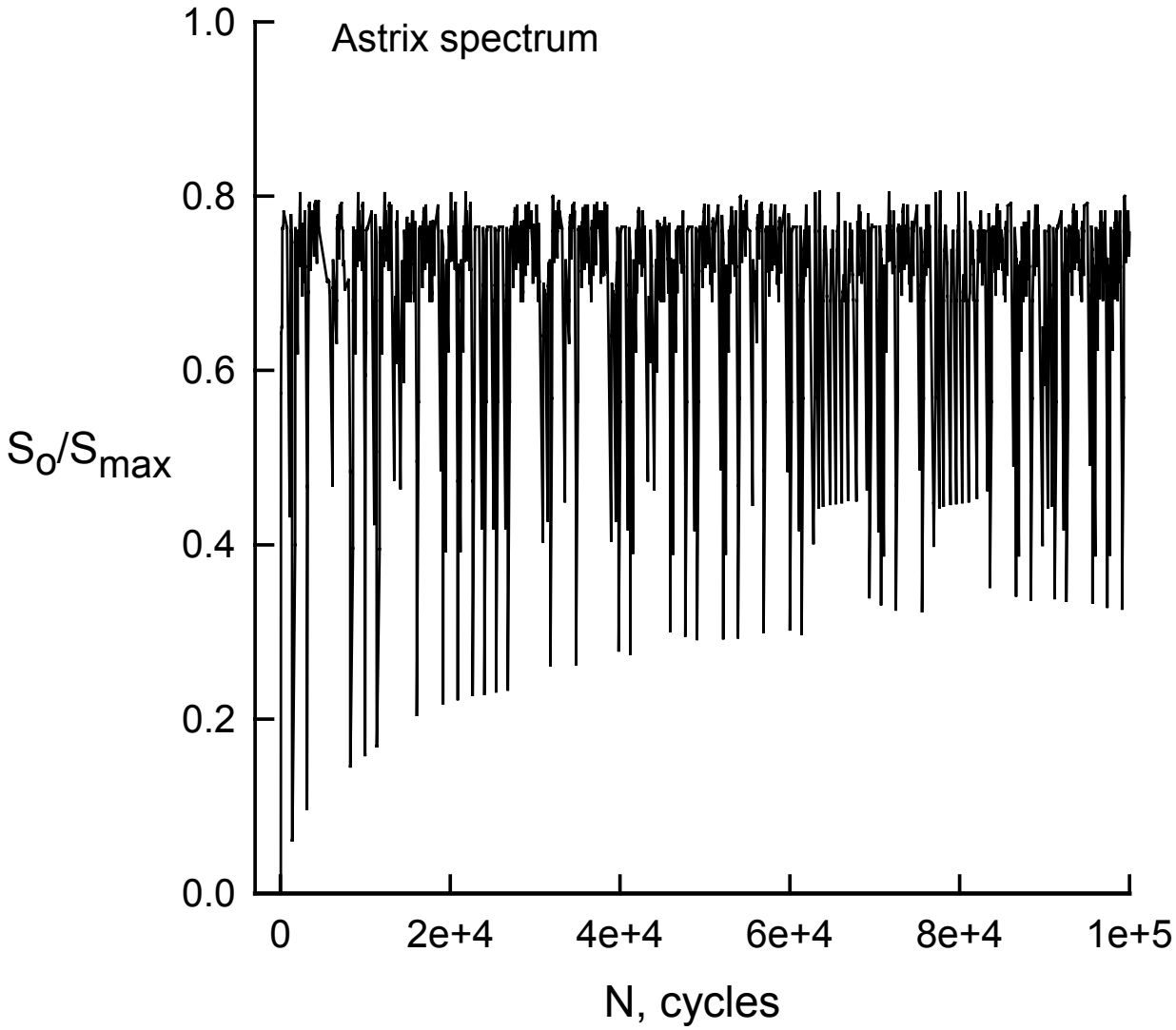

Figure 6(b) – Calculated crack-opening stresses during the application of the Astrix spectrum loading.

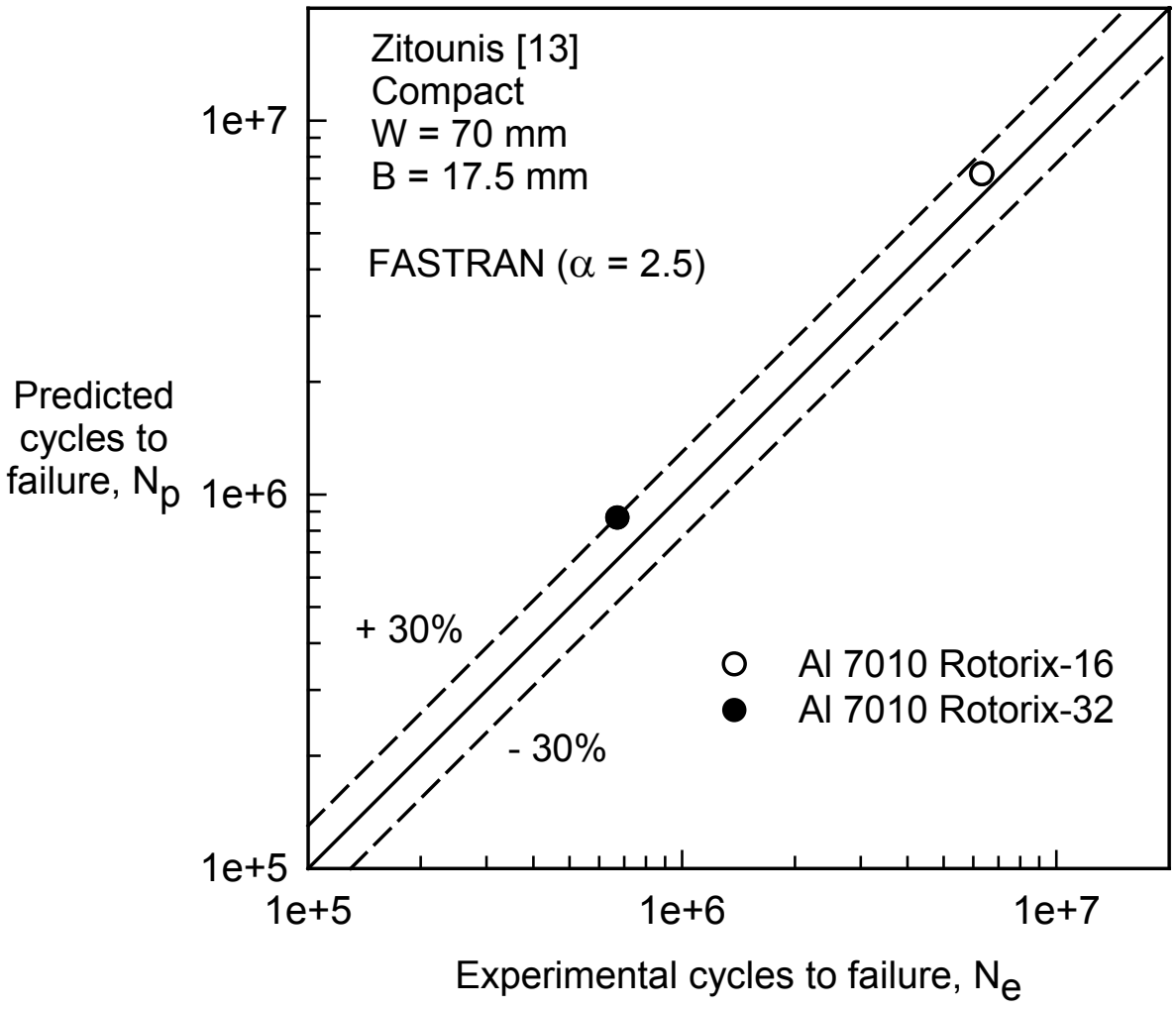

Figure 7 – Measured and predicted crack growth lives in compact specimens under the Rotorix spectrum loading.

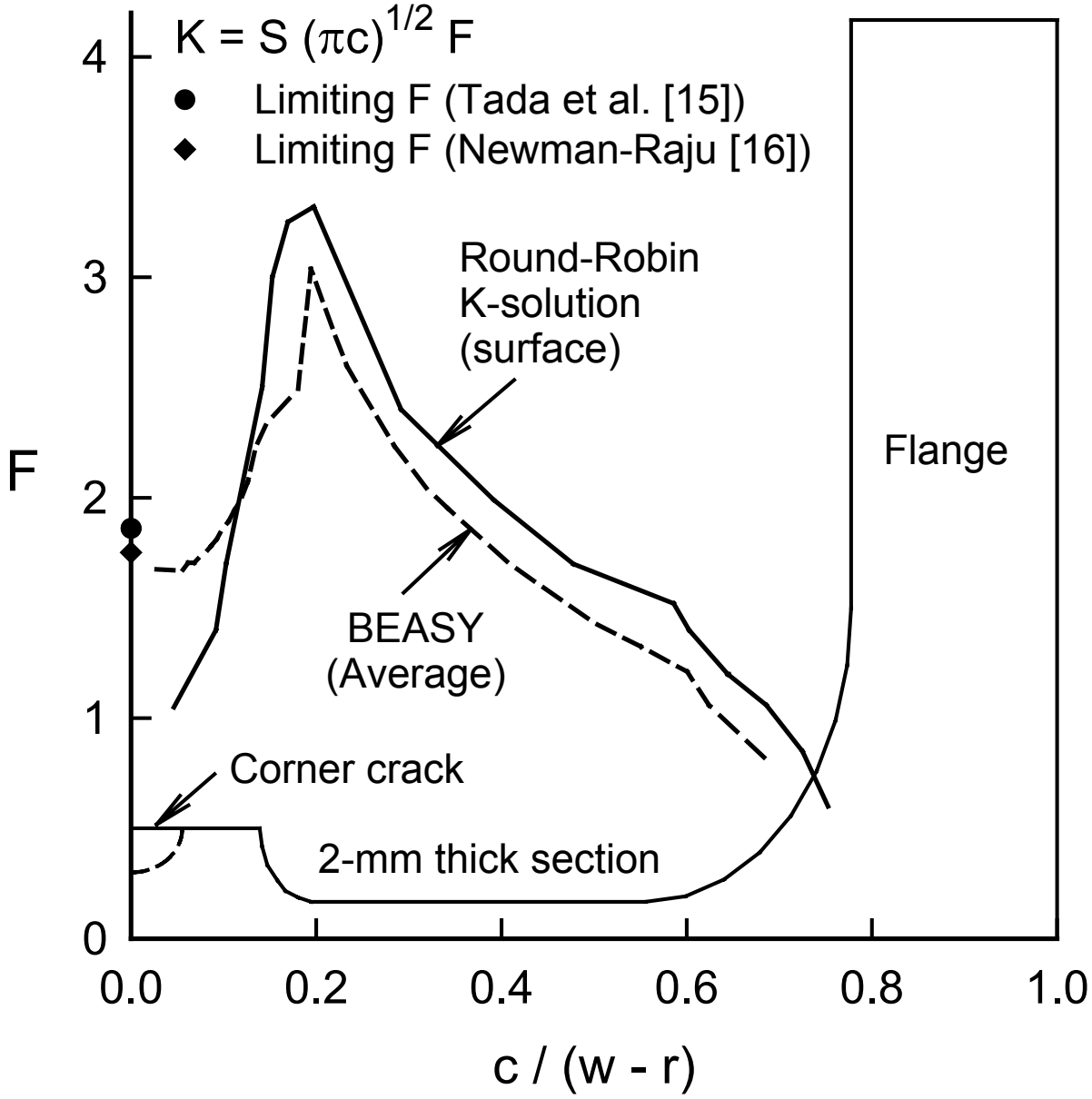

Figure 8 – Stress-intensity factor solutions for round-robin crack configuration as a function of normalized crack length.

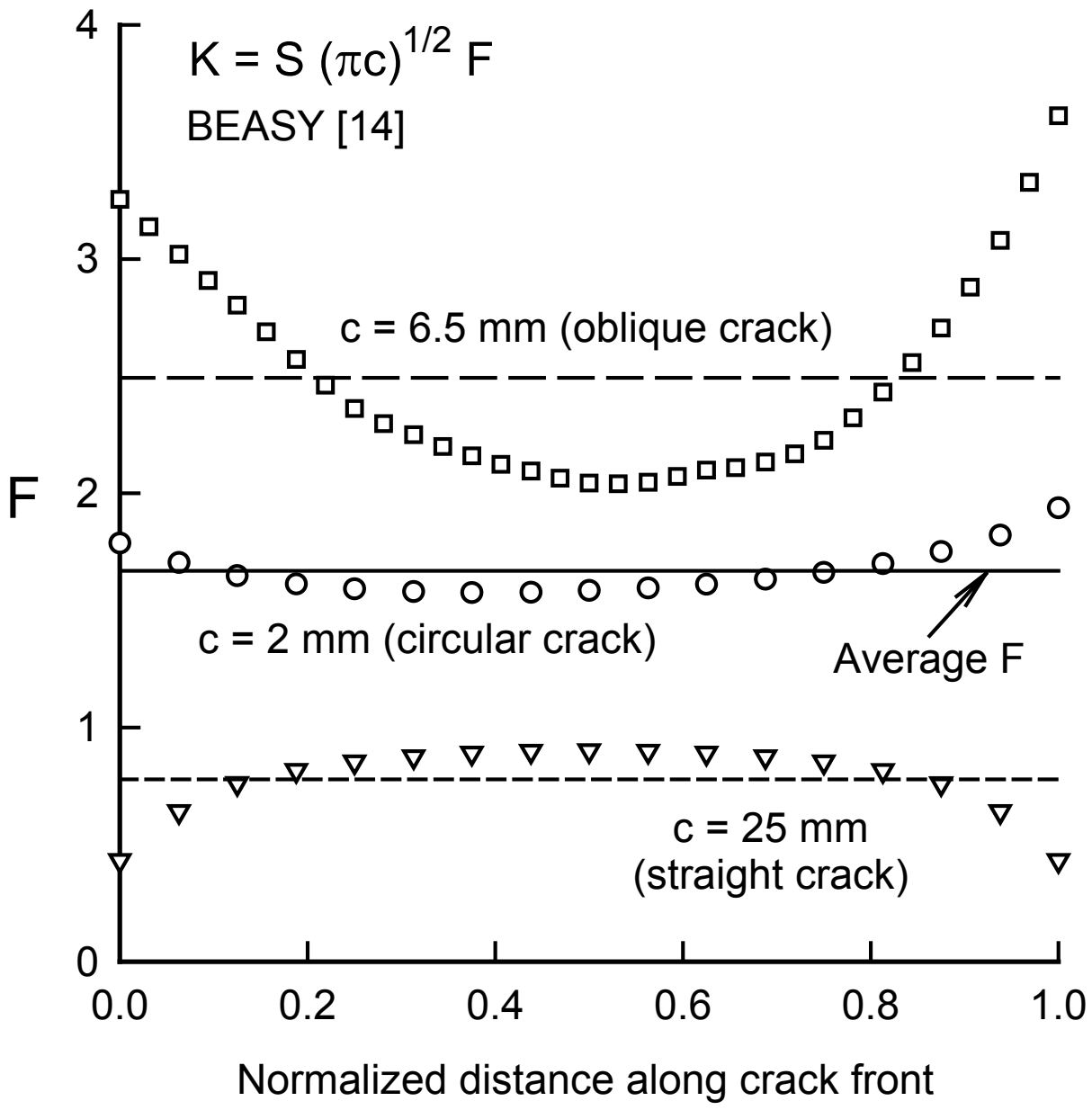

Figure 9 – Distribution of stress-intensity factors along the crack front for various crack lengths in round-robin crack configuration.

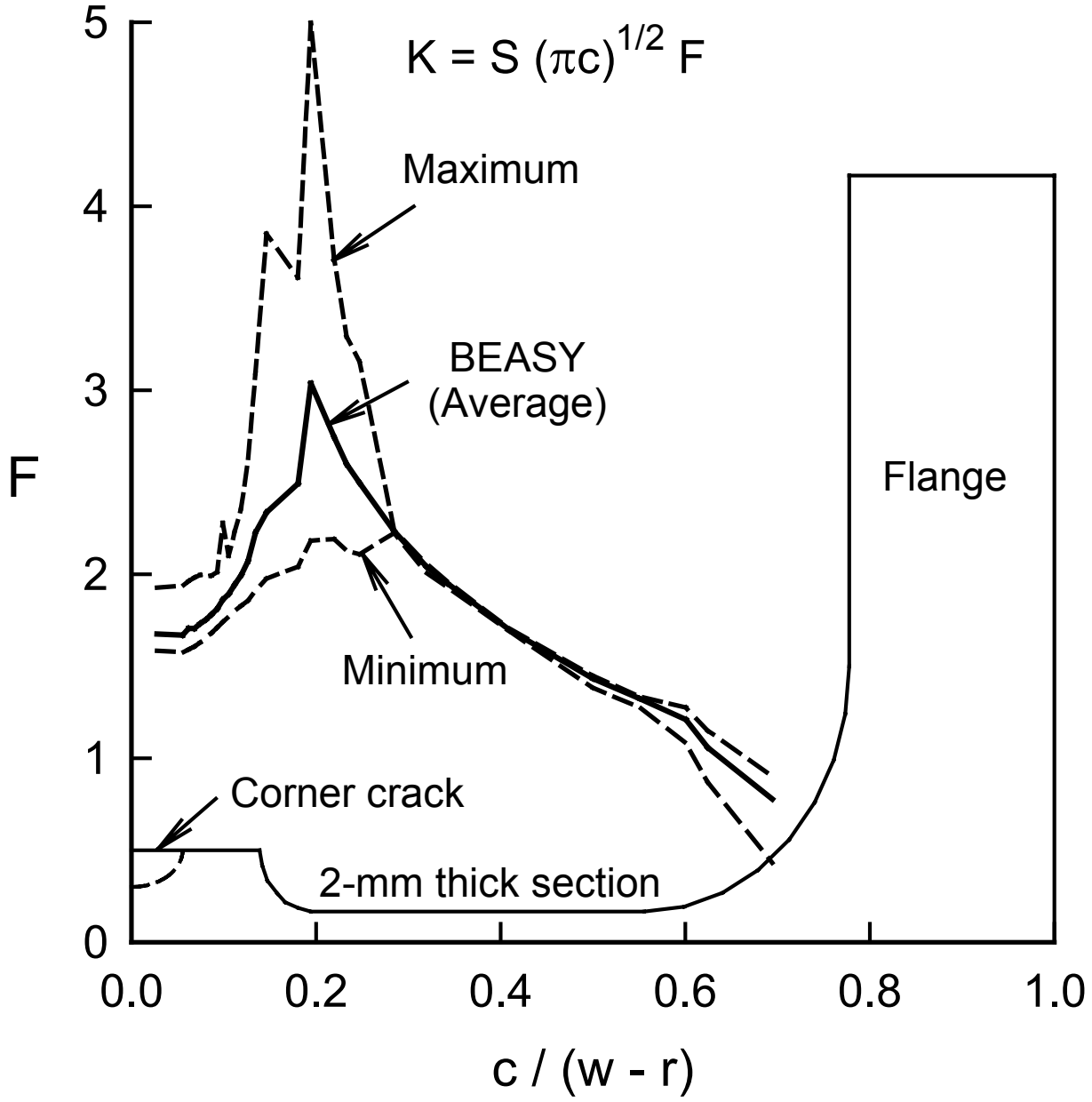

Figure 10 – Maximum, average, and minimum stress-intensity factors from BEASY [14].

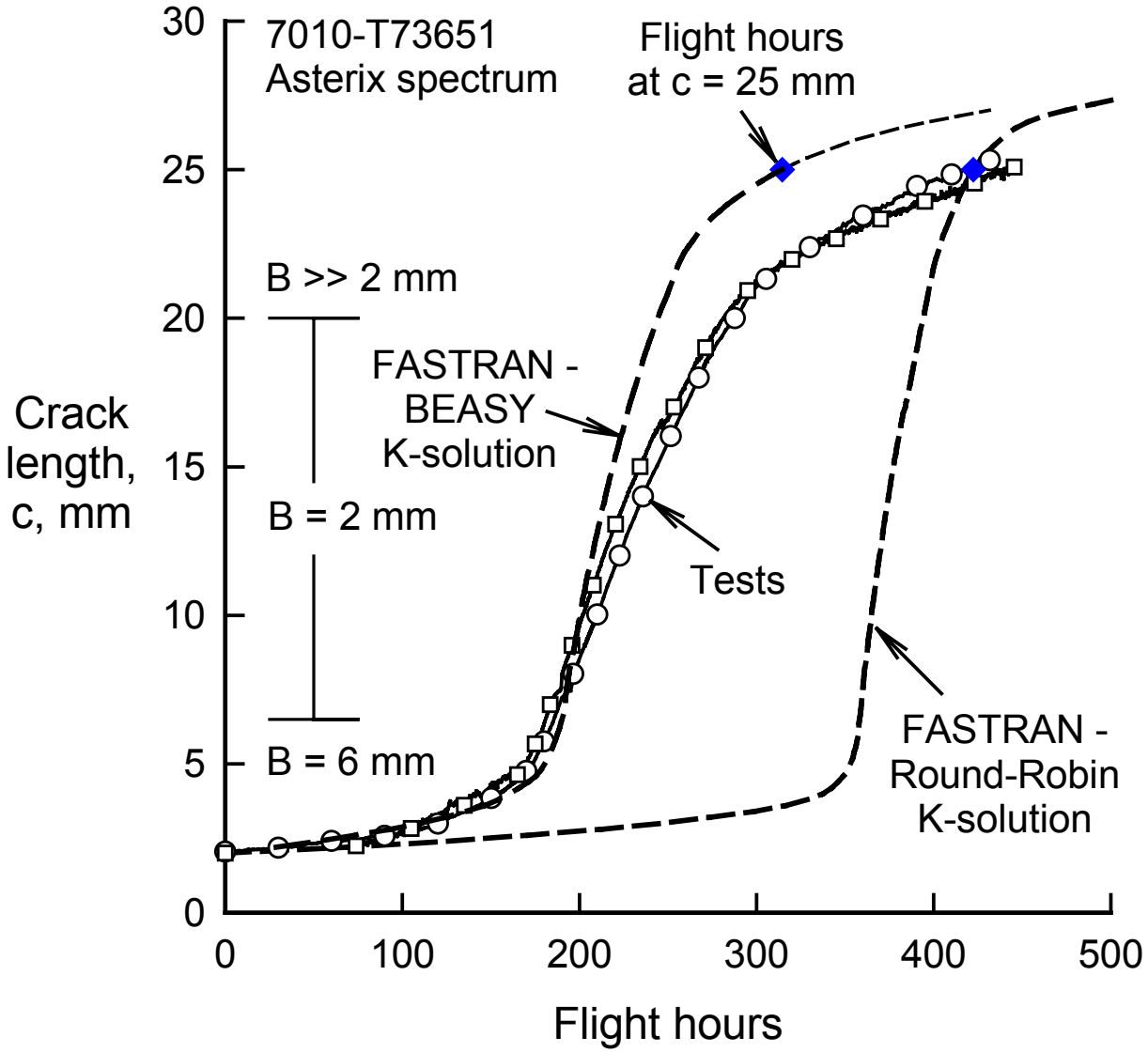

Figure 11 – Measured and predicted crack-length-against-flights for round-robin problem.

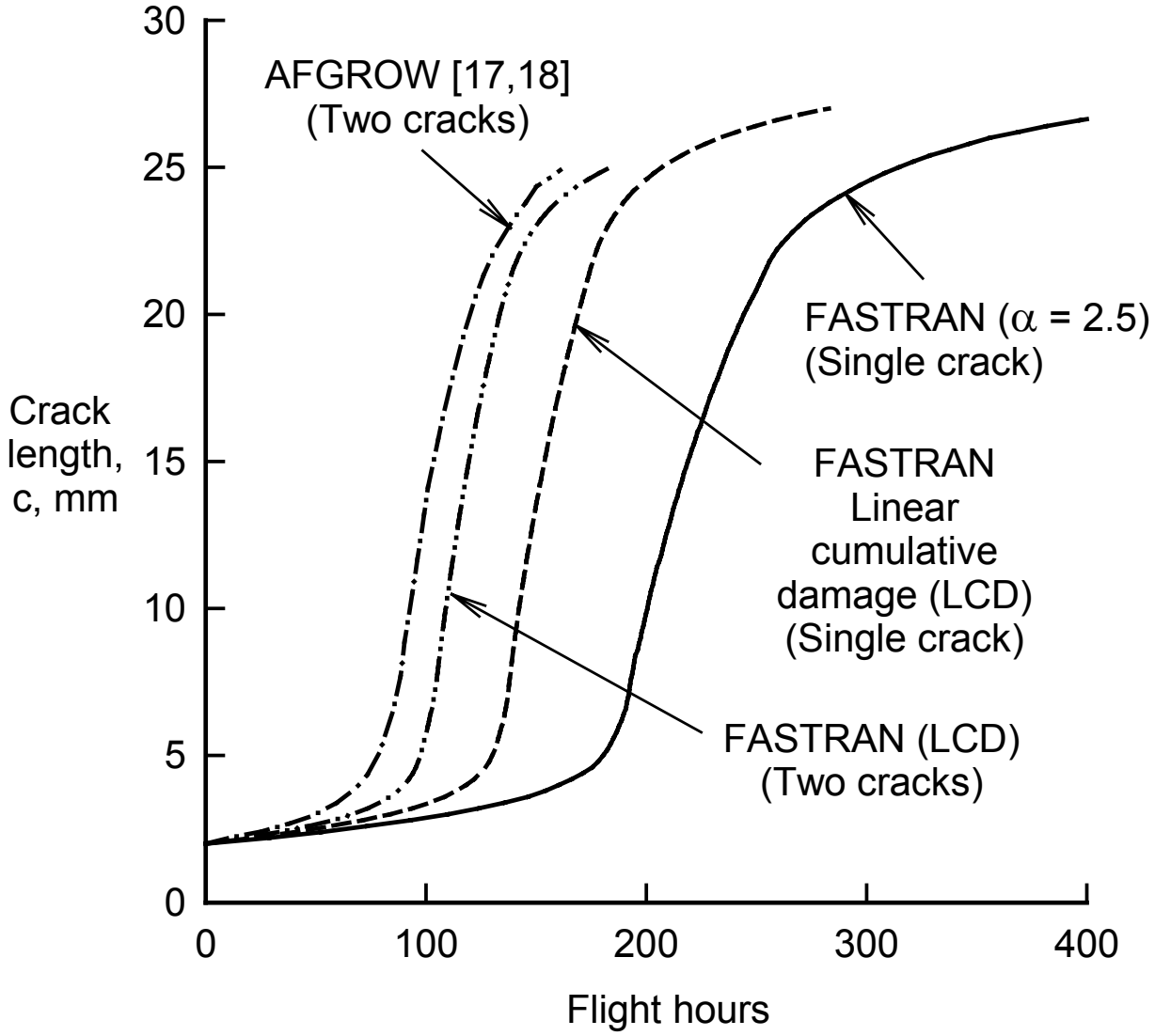

Figure 12 – Comparison of crack-length-against-cycles for round-robin crack configuration using the crack-closure model and linear-cumulative damage calculations.